Estuaries and Coasts
DOI 10.1007/s12237-012-9541-8

Modeling the Hydrodynamic and Morphologic Response of an Estuary Restoration

Douglas A. George · Guy Gelfenbaum · Andrew W. Stevens

Received: 17 November 2011 / Revised: 4 July 2012 / Accepted: 13 July 2012
© Coastal and Estuarine Research Federation 2012

Abstract Estuary evolution is investigated using the hydrodynamic and sediment transport model, Delft3D, to study the response of a dammed tidal basin to restored tidal processes. The development of decadal (10-year) morphological simulations of the restored estuary required simplifying several data inputs and implementing a time-scale acceleration technique. An innovative river sediment discharge schematization was developed that connected sediment discharge to morphological change in the estuary. Mud erodibility parameters were determined from laboratory analysis of sediment cores from the modern lakebed and statistical refinement with a Bayes network of the probability of occurrence. The changing estuary morphology appears to have a dominant impact on the physical habitat (substrate, inundation frequency, mean salinity, and salinity range). The numerical model provides a tool to compare the functions of the historical estuary and possible future alternatives for a restored estuary. Sensitivity of the morphological model to sediment types and erodibility parameters was also examined. A conceptual model covering morphology and indicators of physical habitat for three phases of estuary evolution during restoration is presented that could be applied to estuarine systems that are severely out of equilibrium.

Keywords Estuary restoration · Sediment transport · Morphology · Estuary evolution · Deschutes Estuary · Delft3D

D. A. George · G. Gelfenbaum · A. W. Stevens
United States Geological Survey,
400 Natural Bridges Dr,
Santa Cruz, CA, USA

D. A. George (✉)
ESA PWA,
San Francisco, CA, USA
e-mail: dgeorge@esassoc.com

Introduction

Understanding the physical processes that govern hydrodynamics and morphology of shallow coastal environments is essential to both resource management and restoration efforts. The complex interactions among fluid dynamics, biological activity, sediment transport, and physical changes to the substrate and shoreline create a feedback cycle. Roberts et al. (2000) discussed the concept of equilibrium for intertidal mud flats through time and surmised that with changing external forces (e.g., sea level rise, engineering works), mud flats and estuaries are constantly adapting. Equal space was given to discussing hydrodynamics and morphodynamics in a summary of the state of research on estuarine processes in Uncles (2002), indicating the need to view all components of the estuary evolutionary cycle evenly. More recent investigations present findings as a synthesis of the feedback cycle (e.g., van der Wegen et al. 2011).

Estuary evolution can be viewed from many perspectives, including sedimentologically or geomorphically. Dalrymple et al. (1992) described estuary evolution for wave- and tide-dominated estuaries as a shift in sediment facies. Williams et al. (2002) analyzed the evolution of channels in restoring marshes in San Francisco Bay and found channels evolved through a process of first deepening and then widening by bank slumping. In both studies, the hydrodynamics are controlled largely by the bathymetry of that environment. For example, the location and depth of morphological features (i.e., channels, shoals, and tidal flats) have a substantial effect on the magnitude and direction of waves and currents. Spatially or temporally varying circulation and sediment transport can cause convergences that deposit sediment in quiescent zones and change the bed surface elevation. High-velocity areas can also be maintained as primary conduits for sediment to other regions of the estuary.

Published online: 05 September 2012

The expansion of computing power and speed through the previous two decades has enabled widespread growth of numerical modeling to understand the estuarine dynamics described above. Short-duration, single dimension (1D) linear modeling has expanded to become long-term (decadal) multidimensional (2D or 3D) structured morphological models. For example, Pritchard et al (2002) extends earlier work by Friedrichs and Aubrey (1996) on modeling intertidal flats by incorporating fluid inertia to better represent mud transport and capture accretion/erosion on the upper elevations of equilibrium profiles. Wood and Widdows (2002) added biotic effects to a 1D morphological model to account for changes to the erodibility of the bed in the Humber Estuary, UK, and characterized the balance between physical processes and biological activity. Lesser et al. (2004) and Roelvink (2006) both advanced morphological modeling with innovative techniques related to tidal inputs and coastal evolution—some of which inspired the methods in this study.

To utilize process-based numerical models, input reduction techniques are necessary regarding hydrology to make mid- to long-term (decadal scale) morphological predictions of estuary evolution with reasonable expenditure of computer resources. These techniques are required to produce model output similar to an "average" year but that can be calculated in a fraction of that time (de Vriend et al. 1993). Input reduction techniques have been used for wave and tidal data (Gelfenbaum et al. 2003) and fluvial inputs (Ganju et al. 2008; van der Wegen et al. 2011). Advancing the idea of recurrence statistics, The Nature Conservancy developed the indicators of hydrologic alteration (IHA) to characterize the intra- and interannual variation in flows, according to the following five characteristics of flow regimes: magnitude of monthly streamflows, magnitude and duration of annual extreme flows, timing of annual extreme flows, frequency and duration of high and low pulses, and rate and frequency of flow changes (Mathews and Richter 2007). However, the IHA method does not provide the necessary fluvial schematization for numerical modeling. This paper presents an approach to deconstruct a long-term hydrographic record and build an input that synchronizes with other estuary forcings for a numerical model of estuary evolution.

Another vital component for numerical modeling of estuaries is the characterization of the substrate erodibility, particularly the fine-grain size classes of clay and silt. Fine-grain sediment erodibility depends on the physical characteristics of the sediment, such as sediment grain size and water content (Postma 1967), and mineralogy as well as biological activity (Jumars and Nowell 1984). Despite collection of bed composition and sediment properties in estuaries around the world, there is no generally agreed upon parameterization for estimating the erodibility of mud for sediment transport calculations. An ideal situation to model erodibility accurately would be to calibrate the model with field data and perform hindcasts of observed morphological change (e.g., van der Wegen et al. 2010). The few site-specific datasets found in the literature is an indication that broadly applicable erodibility coefficients do not exist, although attempts have been made at generalization (i.e., van Rijn 1993).

This paper focuses on a method to predict the morphological response of an artificially created lake bottom to restored tidal and river flood processes. A hydrodynamic and morphological model was developed to predict the changes in physical habitat in a basin called the Deschutes Estuary in Washington State, USA. The morphology and physical processes (circulation and salinity) of the estuary influence each other with subsequent changes to the substrate characteristics (e.g., grain size) as a result of the restored tidal processes. Consequently, the physical habitat is expected to evolve through time after dam removal. Decadal predictions of physical processes and bed evolution in the restored estuary allowed comparison of physical habitat characteristics between the predam and restored estuary. The model is also used to explore two restoration alternatives and to explore the sensitivity to bed sediment characterization. The timescale of morphological change and resulting physical habitat is important to the expected biological response of the restored estuary, which could be conducted by ecological modeling at a later time.

Methods

Study Site

The Deschutes Estuary in southern Puget Sound was dammed in 1951 to create a freshwater reflecting pool below the Washington State Capitol campus and the basin became known as Capitol Lake. The barrier, known as the 5th Avenue Dam, consists of a 5-m high earthen and concrete dam, a 25-m wide tide gate with concrete spillways, and a causeway. The modern lake at the head of Budd Inlet is separated into four distinct but connected basins (Fig. 1). The waterbody lies on a north–south axis with the Deschutes River entering from the south; a municipal marina is directly northeast of the dam and the Port of Olympia is north of the marina. As early as the 1970s, accumulation of sediment in the lake from the Deschutes River was identified as a problem to the long-term health of Capitol Lake and portions of the lake were dredged in 1979 and 1986. Comparison of bathymetry from 1949 to 2005 reveal that 1.3 million m^3 of sediment has accumulated inside the lake for an average deposition of approximately 23,000 m^3/year.

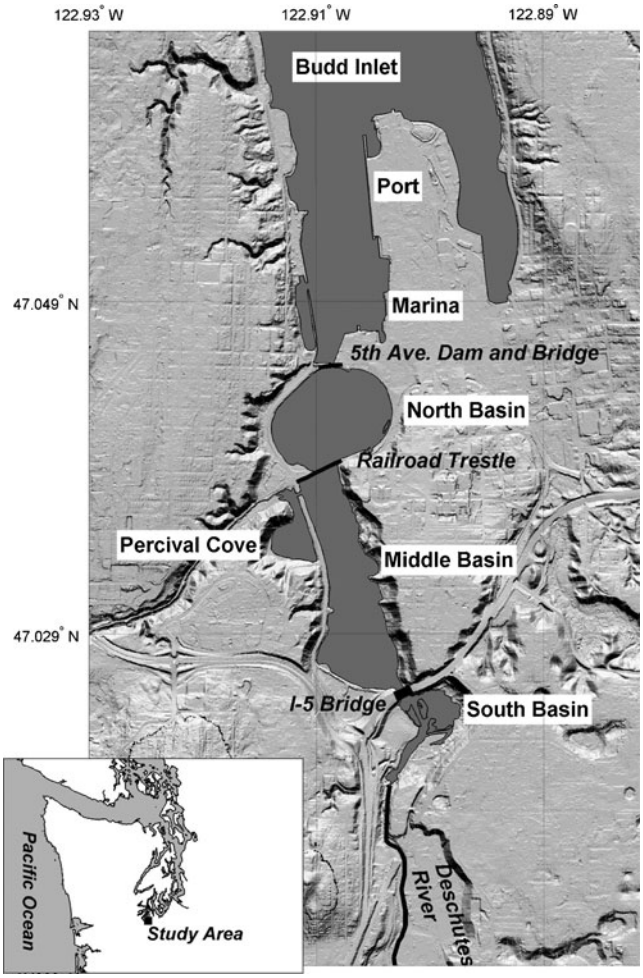

Fig. 1 Map showing Capitol Lake in 2004. The four distinct sub-basins are South Basin, Middle Basin, Percival Cove, and North Basin and are connected through the labeled features. The Deschutes River enters South Basin from the southwest. The Port of Olympia and municipal marina reside north of the 5th Avenue Dam and Bridge in Budd Inlet

Numerical Model

Dominant processes to be modeled in the estuary include river flows, tides, and wind-driven waves, and potentially salinity-driven stratification. Sediment observed on the lake bed and in the Deschutes River ranges from clay to gravel so the numerical model also requires multiple sediment grain sizes.

Morphological modeling of restoration scenarios was evaluated with a process-based numerical hydrodynamic and morphologic model, Delft3D. The model solves the equations of motion, conservation of water, and conservation of sediment at each time step, which results in a prediction of coastal hydrodynamics and sediment transport (Lesser et al. 2004). The model also can simulate transport of flocculated sediment by specification of a settling velocity. Different simulations were assembled to model the predam environment and restoration scenarios—an estuary alternative (Fig. 2a) and a dual basin estuary alternative with a freshwater impoundment in the eastern half of a sub-basin that is not subjected to tidal dynamics (Fig. 2b and Table 1).

Model Input

Model Grids

The predam and restored estuary scenarios extend across different geographic areas, which prompted building two slightly different curvilinear grids unique to the simulations. Both grids extend from the mouth of the Deschutes River to outer Budd Inlet with the predam grid larger to accommodate a larger historic estuary (Fig. 3a). Grid cells in the main estuary channels are <10 m in length, while grid cells in outer Budd Inlet are up to 200 m in length (George et al. 2006).

Bathymetry

Bathymetry of the Deschutes Estuary was collected in 1949 prior to construction of the dam. Depth soundings from a 1936 survey of Budd Inlet (NOS survey number H06199) were fused with the estuary data to establish a predam bathymetry. Modern bathymetry and topography for the Capitol Lake area were compiled from several surveys conducted in 2004 and 2005, including echosoundings (Eshleman et al. 2006), sounding poles, and navigation surveys (US Army Corps of Engineers, 2004) (Fig. 3b, c). Topographic elevations lower than 6.1 m (20 ft) were extracted from local topography for inclusion in the model. All bathymetry and topography were adjusted to NGVD29.

The bathymetry data were projected onto the model grids using triangular interpolation. The estuary alternative is the simplest with the dam removed and the entrance to Budd Inlet widened from 25 to 159 m (Fig. 2a). Bathymetry in the area of the removed dam was estimated by extrapolation of field data. All other depths are identical to the modern lake and Budd Inlet bathymetries. For the dual basin estuary alternative, a strip of lake bottom was raised to 4 m (MSL) with a 2:1 slope on the banks to the east of the center of the basin closest to Puget Sound (Fig. 2b). This closed the eastern half of North Basin to estuarine flushing while allowing tidal processes into the three southern basins.

Open Boundaries

The model includes two open boundaries at its northern and southern extents. The northern boundary is forced with tides. Long-term tidal records were extracted from the National Ocean Service water level station at Gull Harbor in eastern Budd Inlet (station number 9446807). Budd Inlet experiences a mixed, semidiurnal tide with a maximum range of 5 m during spring tides. Twelve tidal constituents

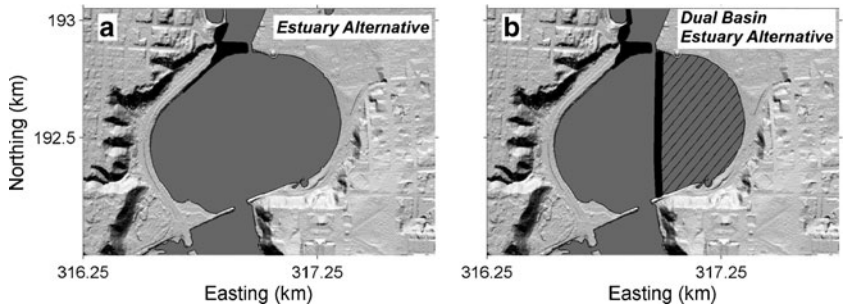

Fig. 2 The two restoration scenarios of **a** estuary alternative and **b** dual basin estuary alternative after removal of the 5th Ave Dam. Both are open to Budd Inlet through a 150-m opening, but the dual basin estuary alternative contains a freshwater impoundment in the eastern half of North Basin, noted as the *hashed section*

were determined to be the dominant contributors to the tide and are used to force the tidal height on the outer boundary of the model (Table 2).

The second open boundary is located at the southern end of the model domain where the 92-km long Deschutes River enters Capitol Lake. The Deschutes River is monitored with several USGS river gauging stations. The gauge closest to the lake, station number 12080010, collected flow measurements from 1945 to 1954, 1957 to 1964 and 1990 to present but contains large gaps within the record. A cumulative record of almost 30 years remains after the gaps are removed. The annual average flow of the Deschutes River is approximately 12 m^3 s^{-1} but fluctuates widely within a year (Fig. 4a). A distinct wet season is observed from November to April with episodic large flood events larger than 100 m^3 s^{-1}. The river flow is approximately 3 m^3 s^{-1} during the dry season, spanning May to October.

The seasonal difference in river behavior heavily impacts the pattern of sediment delivery to the lake. Mih and Orsborn (1974) established that 80–85 % of the annual sediment load arrives by flood events that occur only 8 % of the year. Therefore, even during the wet season, the majority of sediment is not constantly delivered but rather arrives during large flood events. The sediment concentration for different river flows was estimated using a rating curve developed specifically for the Deschutes River (Mih and Orsborn 1974). A total sediment load of 8.6×10^8 kg in 30 years, or an average annual sediment load of 2.87×10^7 kg, was calculated when the river discharge data are applied to the rating curve.

Table 1 Description of simulations used in the hydrodynamic and sediment transport modeling component of the study

Simulation	Description	Modeling goal
Predam estuary	1949 bathymetry and shoreline for Deschutes Estuary, 150 m opening to Budd Inlet	Baseline data for historic environment
Estuary alternative	2004 bathymetry and shoreline of Capitol Lake, 150 m opening to Budd Inlet	Restoration scenario
Dual basin estuary alternative	2004 bathymetry and shoreline of Capitol Lake, 150 m opening to Budd Inlet and freshwater impoundment of eastern North Basin along a north–south axis	Restoration scenario

Input Reduction for Morphological Simulations

Many factors motivated the reduction of complicated time series to enable morphological simulations. Three of the primary drivers were investigating decadal morphological changes to the bed, using small grid cells to resolve tidal channels, and implementing the simulations with a short time step to maintain model stability. To address these factors, the river discharge and input of sediment were schematized and the rate of morphological change was adjusted; both approaches are detailed below.

River Schematization Using the mean flow for modeling the fluvial boundary would not represent the episodic nature of the river. The Deschutes River hydrograph contained 10,806 daily average discharge values over 50 years to enable the construction of a 30-year record to characterize the freshwater and sediment input to the estuary. To simulate the hydrodynamics of the restored estuary for an entire year, the freshwater discharge was binned into five discharge classes based on recurrence intervals. Subsets of actual events were averaged to produce the selected flows and the number of required events was tallied as a percentage of the total (Table 3). When the five river flows are weighted by their respective frequency and combined, the total discharge is equivalent to an annual average calculated from the hydrograph. This schematization was designed for simulations examining hydrodynamics and salinity in the estuary.

The river schematization for sediment transport and morphological change focuses on delivery of similar sediment amounts regardless of the discharge. This helps maintain model stability by reducing large shocks to the simulated environment. The sediment load scales according to the frequency of the river flow, creating a constant delivery of sediment to the estuary. An average sediment flux of 48,800 m^3 $year^{-1}$ was calculated, and five river discharge

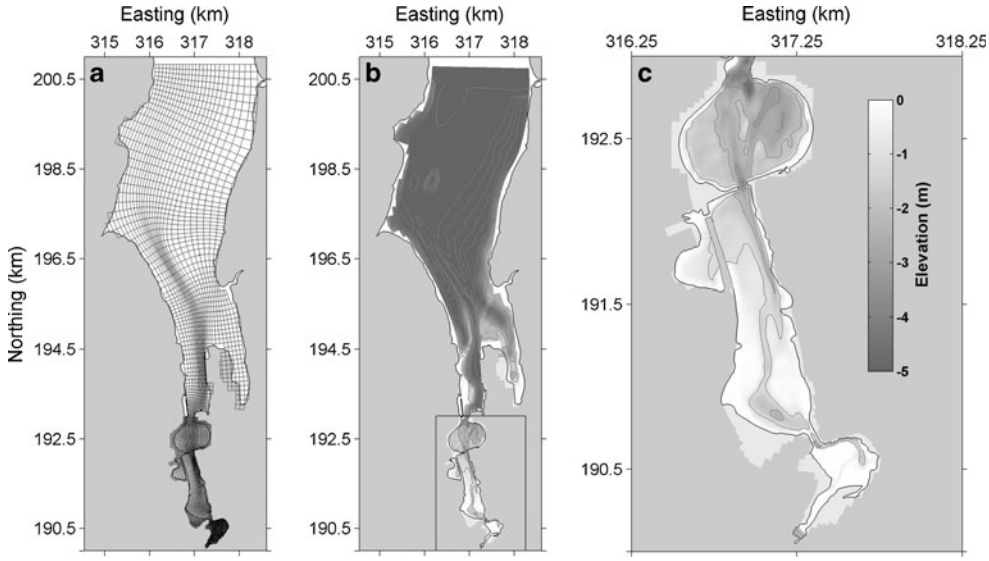

Fig. 3 **a** Numerical model grid, **b** bathymetry for the model domain, and **c** in the modern Capitol Lake region. Grid resolution is higher in the estuary, port region, and ship channel, while other areas have lower resolution. The axes are in Washington State Plane South (km) and bathymetry contours are in 1 m increments

classes were selected using the rating curve to determine the required river flows for sediment delivery. By this technique, the sediment load brought to the estuary in a few large flood events is equal to the sediment load that arrives during small quiescent flows during much longer time periods (Table 4).

Morphological Acceleration Because hydrodynamics respond to changes on short time scales (10–100s of seconds) while morphological changes occur during much longer time scales (10–100s of days), a morphological time scale factor, or MORFAC, was used to scale the morphological change (Lesser et al. 2004; Roelvink 2006). Use of MORFAC also reduces computational time. The scaling occurs by multiplying the depositional and erosional fluxes to and from the bed by the nondimensional MORFAC at every computational time step and incorporating the adjusted bed changes into the hydrodynamic calculations. In a new application designed for this study, MORFAC is applied to the river discharge to scale the amount of sediment delivered in each flood event. In addition, because the river is delivering sediment to the estuary, the river hydrodynamics and sediment load must be linked with the tidal hydrodynamics and morphology (Eq. 1).

$$\mathrm{MORFAC} = \frac{\text{morphological time}}{\text{hydrodynamic time}} = \frac{(\text{days of flow}) \times (\text{minutes/day})}{(\text{minutes in a tidal cycle})} \quad (1)$$

Annual MORFAC values for all river flows are shown in Table 5. Applying MORFAC allows similar percentages of the annual sediment delivery to arrive for each discharge class, but the largest amount still comes from the biggest flow after scaling for flow frequency.

To duplicate the event-driven nature of the river, the five flow classes are arranged as a series of flood events. A flood event is defined as an initial high flow followed by successively lower flows; the low flow effectively "ends" each flood event as the interlude between floods (Fig. 4b). Distinct wet and dry seasons are produced by running the lowest flow five consecutive times after all the flood events are completed. Each flow, except the largest, is included at least twice and therefore, MORFAC values required additional scaling.

For effective model operations, the MORFAC associated with the largest flow in a flood event is used for the duration of that event. For the first event, which begins with 146 $m^3\ s^{-1}$, a MORFAC of 0.78 is applied to all succeeding flows within that flood event (95, 66, 42, and 13 $m^3\ s^{-1}$). This reduces the MORFAC required for the following flood event (beginning with 95 $m^3\ s^{-1}$) so a new MORFAC value is calculated and applied. The MORFAC value shifts halfway through the low flow interlude period to maintain model stability (Fig. 4b).

Table 2 Significant tidal constituents for Budd Inlet

Constituent	Amplitude (m)	Period (h)
M2	1.46	12.42
O1	0.47	25.82
S2	0.35	12.00
Q1	0.07	26.87
P1	0.27	24.07
K1	0.87	23.93
J1	0.05	23.10
N2	0.28	12.66
L2	0.07	12.19
K2	0.10	11.97
M4	0.05	6.21
M6	0.03	4.14

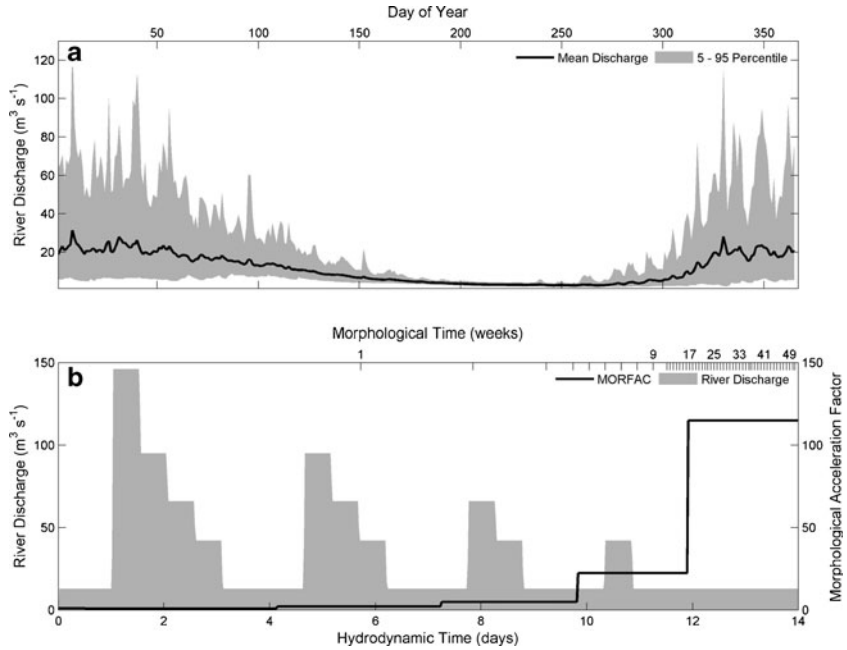

Fig. 4 **a** Daily river discharge range (*gray*) and the daily mean (*black line*) of the Deschutes River over 30 years, showing the episodic nature of the river. Distinct wet and dry seasons can be observed in the hydrographic record. **b** Arrangement of simulated flood events (*gray*) and morphological acceleration factor (*black line*) for sediment transport model runs. An initial high flow is followed by successively lower flows with the average discharge as an interlude between floods. A dry season succeeds the wet season and the entire hydrograph can be repeated to create multiyear simulations. See Table 5 for MORFAC values

The process is repeated four times to generate the wet season sequence. As noted above, the dry season is constructed by five runs of the lowest flow and the dry season MORFAC is scaled appropriately after the last flood event. The final adjusted MORFAC values are used for all simulations involving sediment transport and morphological change (Table 5).

Sediment

Collection and Parameterization of Sediment Grain Sizes

Seventy-two surface sediment grabs were collected in February 2005 from the three basins of Capitol Lake. In general, samples were collected along cross-lake transects to characterize the bed including shallow lakeside regions and primary channels. Protocols for grain size analysis by Sedigraph and settling tubes standardized by the USGS Pacific Coastal and Marine Geology sediment analysis laboratory were followed for all samples except for three, which were deemed to be cobble-sized and required measurement of the individual grains by hand-held calipers (M. Torresan, personal commuication). Sediment grain size statistics and sediment class percentages were then calculated from the data (George et al. 2006).

Grain size distributions of the fluvial sediment load are unknown so sediment from the lakebed was used to reconstruct a probable distribution. Sediment fractions on the lakebed were calculated from the average percentages of the deposited sediment observed from the grab samples (Table 6). The trapping rate for each sediment class was estimated from test simulations of river flow to a modern Capitol Lake (Table 6). By combining the deposited percentage and the trapping rate, the sediment class percentages entering from the river were calculated as 28 % clay, 41 % silt, 28 % sand, and 3 % gravel. The percentage differences for each class are due to the bypassing of the lake by finer sediments. Based on the results from the sediment grain size analysis from the lakebed, mean sediment grain sizes of 2, 31, 200, and 2000 μm were selected to represent four sediment classes for modeling sediment transport. Flux of sediment for each class on the river boundary and interpolated maps of initial bed sediment distribution were produced using these grain size classes. Data from the sediment cores (see below) were also used in the initial bed sediment interpolated maps.

Initial sediment grain size maps were generated only for the estuary region as no sediment data were collected in Budd Inlet. Maps for each sediment class were produced by

Table 3 Discharge classes and occurrence frequency for hydrodynamic schematization

Flow type	Flow (m^3 s^{-1})	Range of flows (m^3 s^{-1})	Daily averages (number)	Time/year (%)
Dry season	2.8	0–3.7	2,994	27.7
Below average	5.6	3.7–8.5	3,016	28.0
Near average	11	8.5–14.5	2,351	21.7
Wet season	24	14.5–45	2,127	19.7
Flood stage	64	45–230	318	2.9

Table 4 Discharge classes, sediment load, and occurrence frequency for sediment transport schematization

Flow type	Flow (m^3 s^{-1})	Sediment load Q_s (kg m^{-3})	Daily averages (number)	Time/year (%)	Days/year (number)
Semidecadal flood	146	1.20	12	0.11	0.4
Biannual flood	95	0.52	43	0.40	1.5
Above average flood	66	0.26	118	1.09	4.0
Average flood	42	0.11	462	4.28	15.6
Near average	13	0.01	10,171	94.12	343.5

interpolating the percentage of the clay, silt, sand, and gravel classes between grab sample locations onto the grid. A fifth map was generated to provide the amount of sediment in terms of thickness at each grid cell location. Most of the bed sediment thickness was set at 10 m to provide sediment in excess of the erosion that was expected. Areas that grab sample data indicated to be coarser than 2,000 μm or where sediment data were not available were "bed hardened" by setting the sediment thickness to 0. These distribution and thickness maps were used as initial bed conditions in simulations of the estuary restoration scenarios only.

Collection and Parameterization of Sediment Erodibility The bulk densities for sand and gravel (1,600 kg m^{-3}) were selected from van Rijn (1993). The erodibility of sand and gravel is well-known and based on relationships such as the Shields curve for determining the critical shear stress for erosion. The erodibility of clay and silt is more difficult to know a priori, as compaction or biological growth can modify erodibility parameters of these cohesive sediments (e.g., Jumars and Nowell 1984). Delft3D uses the Parthenaides (1965) formulation for erosion of cohesive sediment,

$$E = M\left(\frac{\tau_b}{\tau_{cr}} - 1\right) \quad (2)$$

where E is the erosion rate (kg m^{-2} s^{-1}), M is the erosion coefficient (kg m^{-2} s^{-1}), τ_b (Pa) is the bottom shear stress, and τ_{cr} (Pa) is the critical shear stress. The term in the parenthesis is often referred to as the excess shear stress (dimensionless). Both M and τ_{cr} are dependent on the physical and biological characteristics of the bed. Additionally, mass fluxes of sediment are converted to volume using the dry sediment density, which varies according to grain size as well as depositional history (e.g., Stevens et al. 2007). As a result of the large amount of fine-grained, cohesive sediment in the lake, additional field data were required to more accurately represent the sediment properties of fine-grained sediment in the model domain.

Fifteen cores were collected in Middle and North Basins in depths ranging from 0.5 to 3.6 m. The ~0.5-m long cores were capped and shipped upright to maintain undisturbed surface sediment for analysis in a Sedflume Laboratory. Cores were raised into a known flow and subjected to a series of erosion cycles to quantify the erosion rate as a function of shear stress (McNeil et al. 1996; Roberts et al. 1998; Stevens et al. 2008). After each erosion cycle, a physical sample was taken from the core, and the physical properties of the sediment (grain size and dry sediment density) were determined. Erosion cycles were repeated with depth in the core resulting in measurements of τ_{cr}, grain size, and sediment density at ~5-cm depth intervals.

The erosion rate parameter for each erosion cycle was calculated by linear regression between measured erosion rates and excess shear stress (Eq. 2). Measured erosion rates do not generally fit the linear model described by Partheniades (1965) over the entire range of applied excess shear stress (Fig. 5). At high shear stress (τ_b>1.6 Pa), sediment erosion rates in the experimental data were better described by a power law relationship (e.g., Roberts et al. 1998). Rather than attempt to modify the sediment transport formulation in Delft3D, the erosion rate parameter was calculated in the range of excess shear stresses where the linear model was valid.

Erodibility parameters measured on cores vary between cores and vertically with depth in the core (Fig. 6). No clear patterns in dry sediment density, critical shear stress, or

Table 5 MORFAC and sediment volume associated with simulated river flows

Flow (m^3 s^{-1})	Original MORFAC	Scaled MORFAC	Volume (m^3)	Total sediment delivery (%)
146	0.78	0.78	10,400	21
95	2.82	2.05	10,800	22
66	7.69	4.87	10,100	21
42	30.2	22.5	9,900	20
13	664	114	7,600	16
total			48,800	100

Table 6 Percent deposition, trapping rate, and percent flux at the river boundary of selected sediment grain size classes

Sediment grain size (μm)	Deposited in lake (%)	Trapping rate	River boundary flux (%)
2 (clay)	15	0.45	28
31 (silt)	48	0.97	41
200 (sand)	33	1.00	28
2000 (gravel)	3	1.00	3

erosion rate parameter are observed for the cores collected in the lake. However, in several cores, the lowest erosion thresholds and dry sediment densities are near the sediment–water interface, while in deeper layers of the core, more stress is required to initiate erosion of denser sediment. Due to a lack of strong spatial pattern of erodibility parameters, mean values of critical shear stress, erosion rate parameter and dry sediment density for all samples with sand contents <40 % (Table 7) were applied uniformly over the entire model domain.

Wind, Waves, and Bottom Roughness

Both fine grain sediment and sand can be resuspended due to wave activity, which prompted incorporating a simplified wind-driven wave field into the hydrodynamic and morphological model. Capitol Lake is largely protected from wind waves and storms that come from the south so a constant wind field of 5 ms^{-1} from the south was constructed based on averaged data from Deerfield Park/Tolmie State Park in Olympia. A uniform wave field ($H_{1/3}$=10 cm; T_s=2 s) was built from test simulations of the lake. Wave height was automatically reduced in very shallow areas where even small waves would be expected to break. Bottom roughness was set to 65 $m^{1/2}$ s^{-1} in the *u* and *v* directions (Chèzy formulation).

For wave-enhanced bed shear stress, Delft3D addresses the nonlinear relationship between waves and currents through a suite of wave–current interaction models. The parameterization developed by Soulsby et al. (1993) is used for model simulations involving sediment transport in two dimensions. The effect of the basin's shallow depths on the combined shear stress from waves and currents prompted a comparison between simulations with and without waves. Waves were found to contribute <0.5 % to total shear stress when water depths were deeper than 0.5 m. In locations on the mudflats that occasionally became very shallow (or eventually dry), the percentage contributed by waves increased, but the overall effect on sediment transport was determined to be negligible because of the absence of currents to move sediment.

Modeling Approach

Initial model simulations revealed salinity-induced vertical stratification inside the restored estuary (differences of <5 psu from surface to bottom). The stratification was just enough to warrant dedicated three-dimensional hydrodynamic simulations first with a static bed and then with an evolved bed from the morphological model. The 3D model simulations used uniformly spaced seven-layer vertical domains, a 2.4-s time step and were forced with a complex tide comprised of the dominant tidal components and the river schematization designed for hydrodynamic modeling. A salinity of 28 was used in Budd Inlet and freshwater in the Deschutes River. These simulations were run for 2 weeks (the spring–neap tidal cycle) for each river discharge class then scaled and summed to represent a full year.

Despite the need for 3D model simulations for hydrodynamics, the computational expense for 3D sediment transport and morphological simulations proved to be excessive and prohibitively long. The estuary was determined to be well-mixed enough for sediment transport so the morphological model runs were operated in 2D with a 6-s time step for the two restoration alternatives but not the predam scenarios. A simplified tide was used to remove the need to simulate the complex semidiurnal inequality during the spring-neap tidal cycle (Latteux 1995; Gelfenbaum et al. 2003). The amplitude of the largest component, M2, was

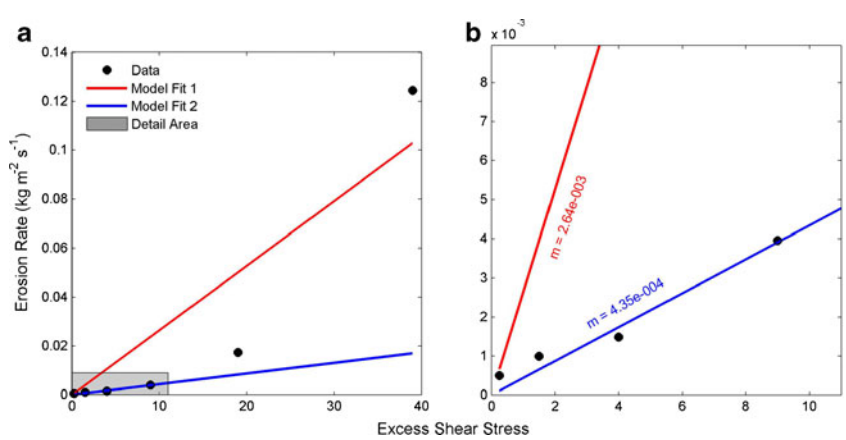

Fig. 5 Example fit of the measured erosion rates to the model of Partheniades (1965) showing **a** a poor fit over the entire range of excess shear stress and **b** a better fit to the linear model if the data are limited to the lower range of excess shear stress

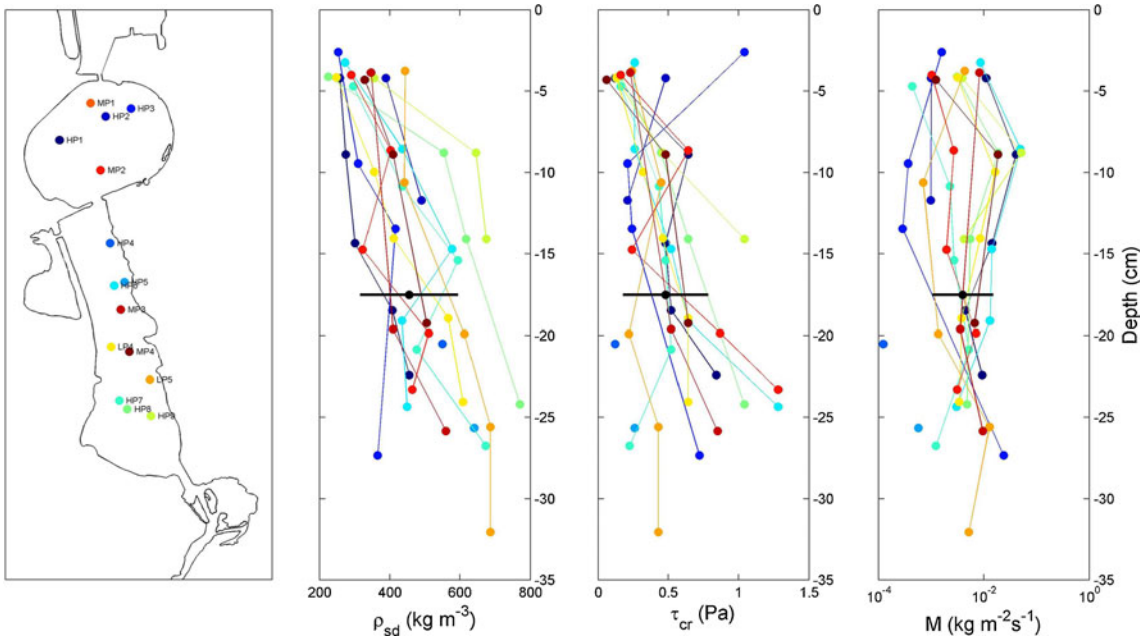

Fig. 6 Down-core patterns in dry sediment density, critical shear stress, and erosion rate parameter for each core collected from Capitol Lake. Samples with >40% sand content were removed from the plot

multiplied by 1.1 and a harmonic "morphological tide" was generated for tidal forcing. Fluvial forcing included the four sediment size classes and associated sediment concentrations. Underlying stratigraphy was used in all simulations to track the evolution of the bed sediment grain size through time. Delft3D simulates flocculation of fine-grain sediment with a user-defined maximum settling velocity for flocs dependent on a user-defined salinity value at which complete flocculation occurs, which were set at 0.001 m s^{-1} (Hill 1998) and 10, respectively. The constant wind and wave fields were included for all simulations.

Results

The process-based morphological model is a powerful tool to understand the course of estuary evolution, examine the behavior of the restored estuary, and differentiate among restoration scenarios. The bathymetry, sediment grain size on the estuary bed, inundation frequency, and near-bed salinity comprise the physical habitat of the estuary. Along with the volume of sediment eroded and deposited, these physical habitat metrics characterize the evolution of the restored estuary for a period of 10 years after dam removal.

Estuary Alternative

Tidal processes will be restored to the estuary immediately after dam removal, and the bathymetry and surface sediment will respond to new hydrodynamic conditions with morphological changes. The model results for the estuary alternative show widespread erosion and deposition patterns that result in a deepening of the Deschutes Estuary after 10 years (Fig. 7). Erosion ranges 0.5–2 m throughout the estuary, with the removal of the elevated mudbanks accounting for the majority of the mobilized sediment. The channels and constriction points also erode where they are not bed hardened. Depositional patterns

Table 7 Sediment characteristics and erodibility parameters from Sedflume analysis including mean grain size, sand content, dry sediment density, critical shear stress, and erosion coefficient: only results from samples with sand contents <40 % are shown (n=52)

Parameter	Mean	SD	Min	Max
Mean grain size (μm)	23.6	7.2	13.8	41.3
Sand content (%)	20.8	8.1	8.5	38.3
Dry sediment density (kg m^{-3})	454.9	138.6	224.7	770.6
Critical shear stress (Pa)	0.48	0.30	0.06	1.28
Erosion coefficient (kg m^{-2} s^{-1})[a]	0.0039	3.7019	0.0001	0.0508

[a] The geometric mean and standard deviation are reported for the erosion coefficient

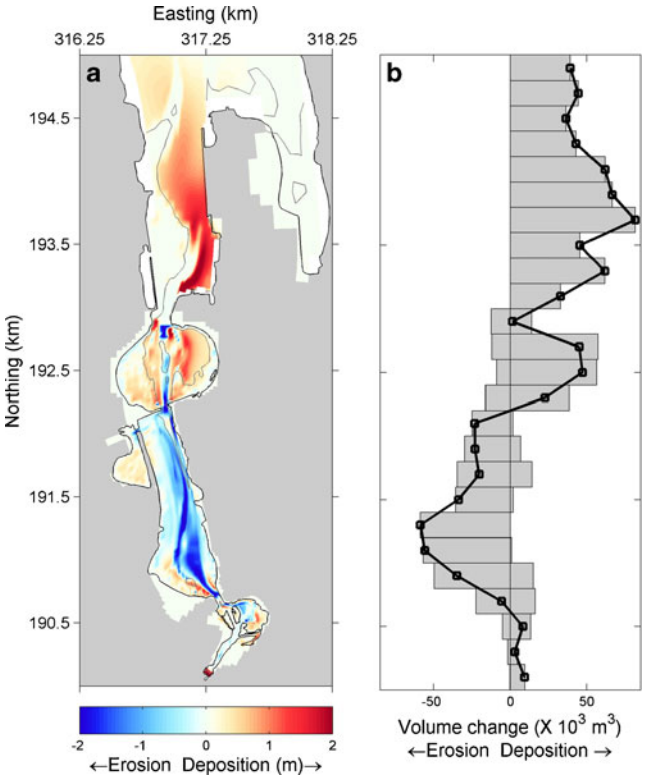

Fig. 7 **a** Erosion and deposition for the restored estuary 10 years after dam removal. *Blues* indicate erosion, and *reds* show deposition. Middle Basin experiences the most widespread erosion, while North Basin and the region outside of the estuary accumulate sediment. **b** Volume change through different segments of the estuary

indicate a large export of sediment from the estuary, but noticeable amounts of accretion (up to 1 m thick) occur in deeper sections inside the estuary. Sediment also accumulates in small depressions through the estuary. Despite the deposition, the estuary is eroded more than it accretes, which results in a net volume increase of 2.0×10^5 m^3.

The annual average near-bed salinity shows a steady gradient from freshwater on the river boundary to a brackish and marine environment at the estuary mouth (Fig. 8a). The near-bed salinity shows an annual average maximum of ~25. In addition, little vertical stratification is observed inside the estuary when comparing surface and bed level salinity, indicating a mostly well-mixed system. The constriction points control the average salinity regimes, with progressively more saline environments downstream from the river boundary. In addition, the channels are slightly fresher on average, which is likely due to constant river flow during the lower stages of the tide. During higher river flows and flood events, the estuary becomes fully flushed with fresh water; conversely, during low river flow periods, the estuary is more saline.

The inundation fraction per annum, calculated by combining inundation results from the five river flows over a 2-week spring–neap tidal cycle and scaling up to represent 1 year, shows an estuary that is submerged a majority of the year (Fig. 8b). Most of the area in the deeper basins is inundated more than 70 % of the time, with the main channel underwater nearly 100 % of the year. Banks on the sides of the basin and large intertidal areas near the river mouth are exposed >50 % of the year with some portions of the islands rarely underwater. The inundation fraction is more controlled by the tidal stage than the river flow, although water levels are higher when extreme river events occur during high spring tides.

The patterns of grain size distribution on the bed shift during the morphological changes in the estuary during 10 years of the simulation. The initial distributions, built from the surface grabs and cores, show sand concentrations to be largest in high-energy areas (channels, constriction points) and mud concentrations on the flanks (Fig. 9a, b). The estuary is dominated by sandy silt, clayey silt, and sand (Fig. 9c, Table 8). After 10 years, the high energy areas remain predominately sandy bottom, but the amount of sand has increased (Fig. 9d). The sand fraction is larger than 0.75 in the channels with some locations exclusively sand. Elsewhere, however, the sand content is negligible and mud dominates the substrate in deeper depressions, backwater areas, and flanks off the main channel (Fig. 9e). More than 80 % of the evolved estuary bed can be described as sandy, silty sand, sandy silt, and silt (Fig. 9f, Table 8).

Dual Basin Estuary Alternative

In general, the dual basin estuary alternative behaves similarly to the estuary alternative with differences observed from the modifications specific to this scenario. With the retaining wall along a north–south axis blocking tidal processes in the eastern half of North Basin, the primary channel does not meander or bifurcate but rather runs parallel to the retaining wall. The channel achieves a depth of approximately 3 m and maintains a sand-dominated substrate. With most of the flow adjacent to the retaining wall, North Basin exhibits slightly slower velocities and without the counterclockwise eddy in the eastern half of the basin during flooding tides. The inundation fraction is similar as are the mean near-bed salinity and salinity range, although with some slight freshening along the retaining wall in North Basin. The amount of sediment eroded inside the estuary is larger (approximately 50 % initially) because the eastern half of North Basin is closed off from any sediment transport pathways, which prevents deposition of material. As the simulations extended beyond 5 years, the differences in sediment transport reduce to <10 %.

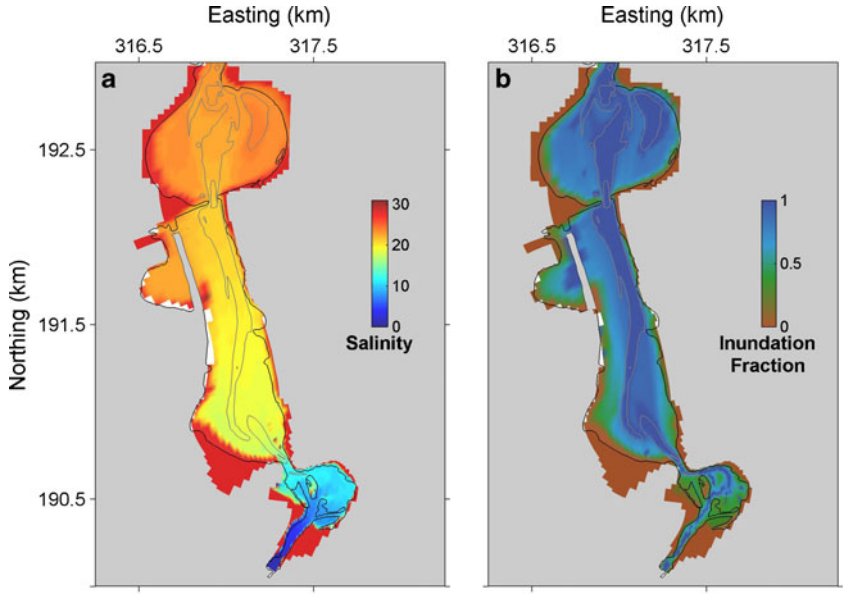

Fig. 8 Modeled (**a**) annual near-bed salinity and (**b**) annual mean inundation fraction conditions in the estuary 10 years after dam. The hydrodynamic simulations were performed on the evolved bathymetry. For mean salinity, *blues* indicate freshwater and reds show highly saline water. For inundation, *blues* indicate continuous submersion and browns show continuous exposure

Discussion

Comparison of Evolved Restored Estuaries to the Historical Estuary

The conceptual model that guided this study focused on understanding some of the tenets regarding estuary evolution: hydrodynamics, sediment transport, and morphology. Returning tidal processes to a system out of equilibrium, such as a dammed tidal basin, allows the investigation of estuary evolution through the perspective of restoration. The goal of restoration science is often not to recreate a historic environment but rather to develop a restored environment with similar processes to the historic one and be self-sustainable. A strong underpinning of restoration work is a realistic perspective that a restored system may resemble but not be identical to the original, unadulterated one (Simenstad et al 2006). The degree to which a restoration, be it

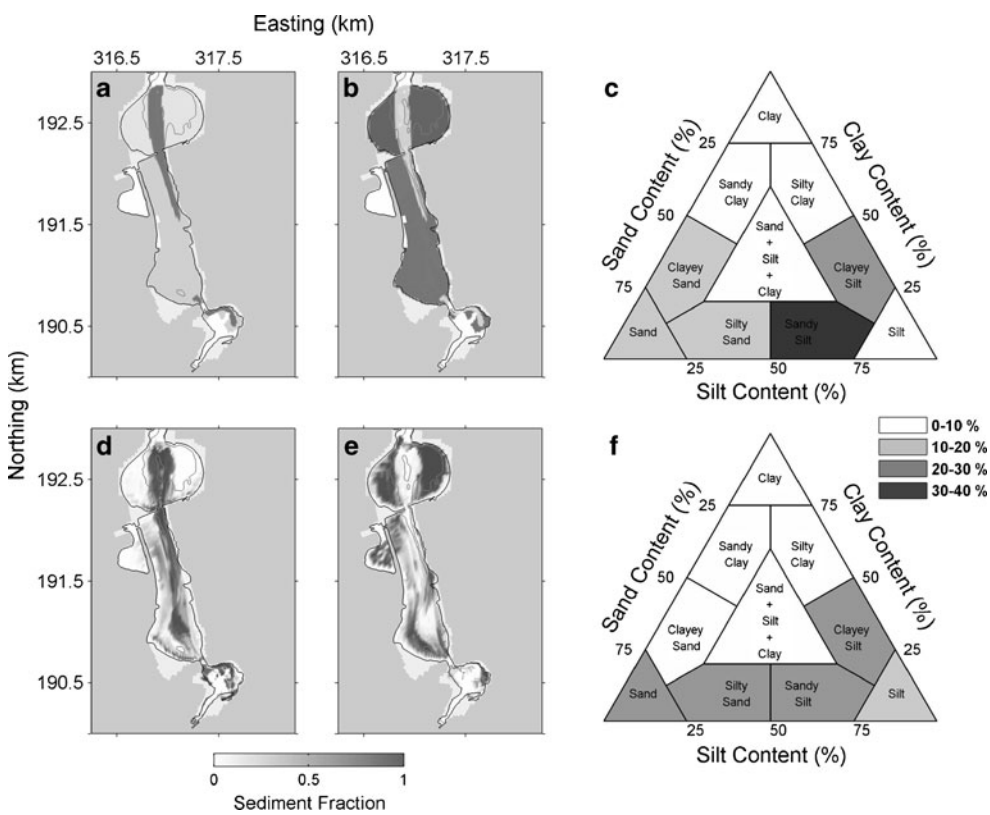

Fig. 9 Initial spatial distributions of **a** sand and **b** mud for sediment transport and morphological simulations. The estuary is dominated by sandy silt, clayey silt, and sand (**c**, see Table 8 for data). Spatial distributions of **d** sand and **e** mud after 10 years. After 10 years, more than 80 % of the evolved estuary bed can be described as sandy, silty sand, sandy silt and silt (**f**, see Table 8 for data)

Table 8 Sediment classes on the estuary bed initially and after 10-year simulations for the restored estuary alternative

Sediment class	Initial percentage	Final percentage
Silty clay	0.00	0.97
Clay	0.00	0.26
Sandy clay	0.00	0.18
Clayey sand	5.73	0.26
Sand	14.46	20.54
Silty sand	5.33	21.07
Sandy silt	47.36	23.97
Silt	0.40	13.70
Clayey silt	22.65	16.59
Sand silt clay	4.39	2.46

actual or simulated, is determined to be successful depends on the objectives of a particular project.

One benefit of forecast numerical modeling is the production of a distinct environment that can be compared to a historical one. After 10 years of simulated estuarine processes and morphologic change, qualitatively the bathymetry of the restored estuaries in this study evolved to be comparable to the bathymetry of the predam estuary and significantly different from the modern lake (Fig. 10). Bifurcated channels and shoals between the channels were similar in the predam and Estuary Alternative estuaries. Although better defined and slightly deeper for the restored estuaries, the primary tidal channel meanders with a similar shape between the historic and restored estuaries. Some areas were shallower in the predam estuary, while anthropogenic alterations permanently affect other portions of the estuary near the river input. Quantitatively, the depth distribution of the restored estuary for both estuary alternative scenarios more closely resembles the depth distribution of the predam estuary than of the present-day lake (Fig. 11). The percentages of surface area for elevations between −5 and 2 m show close similarities for the restored and predam estuaries, particularly for depths > −3 m. The volume of any restored estuary will be smaller than the predam estuary because of the reduced land area available for restoration. Even so, the estuary alternative is closer in total volume to the predam estuary (1.5×10^6 and 1.9×10^6 m^3, respectively) than to the modern lake; the volume of the dual basin estuary alternative is even less than the modern lake due to the freshwater impoundment.

Integrating the bathymetric changes for each sub-basin through time allowed a broader interpretation of how the estuary is evolving and what impact could be expected seaward of the estuary. Initially, large volumes of sediment (100,000–150,000 m^3) were removed from the upper reaches of the estuary and exported to downstream basins and out of the estuary (Fig. 12). The dual basin estuary exports sediment that would accumulate in eastern North Basin, which accounts for larger volume changes. Both estuary alternatives indicate large shifts in the first years after dam removal but gradually decreases through time as the rate of volume change asymptotically approaches the amount of sediment delivered by the river and the estuary moves toward dynamic equilibrium.

Concept of an "Evolved" Estuary

Of the several physical habitat parameters that were investigated—water properties, frequency of wetting and drying, and substrate—the most substantial long-term changes were observed in the morphology of the bed. Therefore, redistribution of sediment should be considered the fundamental shift in physical habitat that affects the response of the other parameters to differing degrees. This is consistent with observations by Dalrymple et al (1992) that tidally dominated estuaries would evolve through progradation of sediment facies seaward. If morphological change is considered the measure of an evolving estuary, understanding how this parameter shifts through time provides a gauge of how quickly the estuary as a whole would transform. The spatial pattern of annual bathymetric change revealed that the largest changes occur in the first year after dam removal. Morphological changes will affect intertidal areas as erosion decreases elevations below the higher tidal stages. Conversely, inundation frequency in regions of deposition may not change substantially if not enough sediment accumulates to elevate these areas above the tides. The salinity regime would be expected to respond to a deepening environment by a narrowing of salinity ranges and an increase in mean near-bed salinity due to more prolonged inundation by marine waters. The mobility of the finer-grain size sediment found in a human-impounded estuary would determine shifts in the substrate but a general coarsening of the bed should be expected as mud is exported during the first stages of estuary evolution.

The rates at which these processes evolve the estuary are not constant. Three stages can be identified according to the rate of morphological change and the response of other physical habitat parameters (Fig. 13). High flow events would be pivotal through all stages to increase the bed shear stress and mobilize sediment. The first stage, initial shift, involves a leveling of the estuary bed, with erosion of unsupported mud banks and deposition in available depressions. The rate of morphological change and substrate type shifts is rapid, as is the expansion of frequently inundated areas; the salinity regime is transitioning toward a more saline brackish composition. The next stage, restoring estuary, can be described as diminishing rates of change from the first stage but a continuation of the general sediment rearrangement, expansion of wet areas, and adjustments to the salinity regime. The estuary is responding positively to

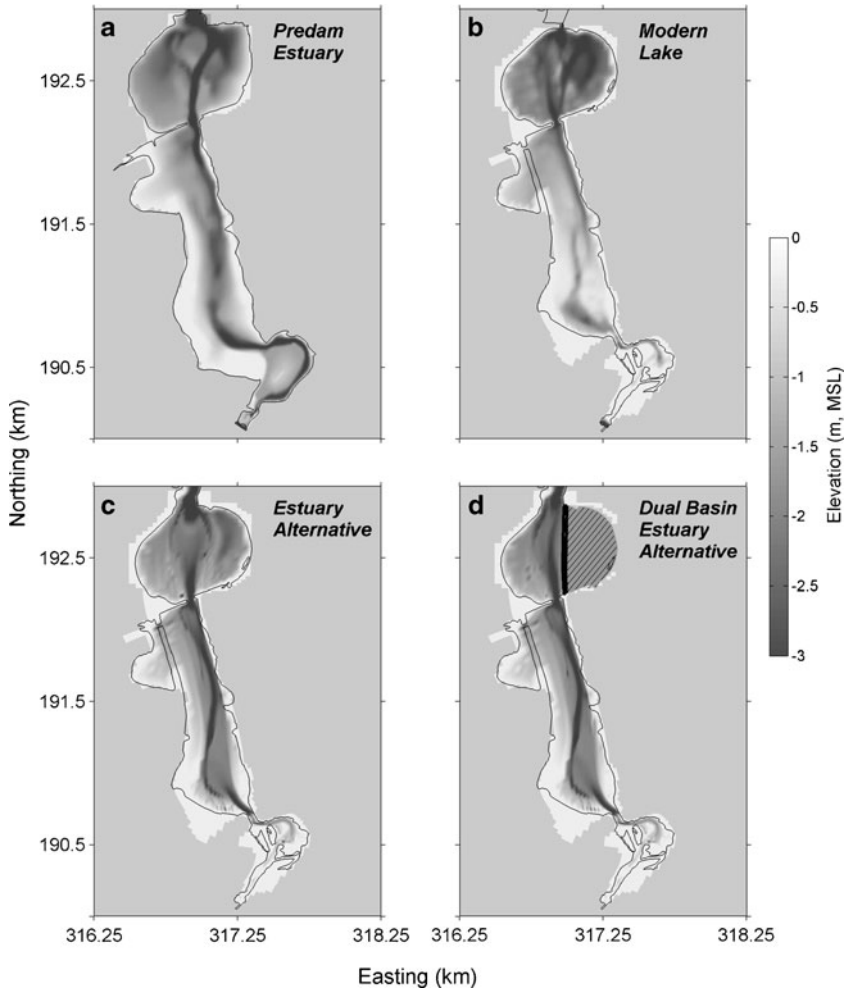

Fig. 10 Bathymetry of the Deschutes Estuary **a** in the predam stage, **b** current Capitol Lake, **c** 10 years after dam removal for the Estuary alternative, and **d** 10 years after dam removal for the dual basin estuary alternative. Bathymetry contours are in 1-m increments. Qualitatively, the simulated estuary results show a similar evolved bathymetry as the predam environment

the return of tidal dynamics. The third stage is dynamic equilibrium and portrays the estuary in a maturing stage where erosion of unsustainable high elevations continues but accumulation of river sediment has begun. Rates of change are small for all of the physical habitat properties but, due to continued supply of sediment from the river, the estuary will continue to adjust. New conditions, such as climate change, sea level rise, or catastrophic events will also cause estuary adjustment. The phases of estuary evolution are not bound by discrete years. The initial shift would be expected to be the shortest in longevity of the stages, while the length of time for restoring estuary would depend on the degree of repair necessary for a particular estuary.

The three stage concept supports the work of Sondi et al. (1995) on environments described as "disequilibrium" estuaries, or those that exhibit a gradual increase in sediment volume contained within the estuary. The restored estuary also fits well into the classification of estuary evolution proposed by Dalrymple et al. (1992) with progressive infilling of a tide-dominated estuary developing into a tide-dominated delta. Estuaries are in a state of flux as they respond to the input of sediment, flood events, sea level change, and tectonic activity (Davis 1978; Cooper 2002), so readjustment after significant anthropogenic perturbations should also be expected to occur.

Model Uncertainty and Limitations

Predictions of sediment transport in general, and specifically long-term predictions of mud transport and morphological change, contain many uncertainties. Haff (1996) categorized seven sources of uncertainty for geomorphic modeling as model imperfection, omission of important processes, lack of knowledge of initial conditions, sensitivity to initial conditions, unresolved heterogeneity, occurrence of external forcing, and inapplicability of the factor of safety concept. Several techniques were employed to limit or at least characterize these uncertainties and data shortcomings. Compromises made during model design and operation and limitations from field observations must be understood to retain confidence in the simulation results.

The limitations for this modeling effort fall into two of the Haff (1996) categories. The first is model imperfection: design and operation. One of the largest limitations in this group is

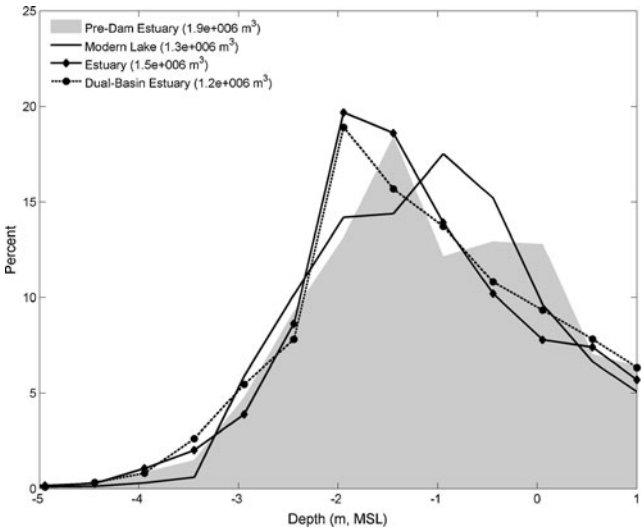

Fig. 11 Distribution of percentages of depths for the predam estuary, the modern lake and the two restoration alternatives. The predam estuary and restored estuaries show similar depth distributions deeper than −1 m MSL, while the modern lake is generally shallower than any of the estuaries. One notable difference is the prevalence of depths that correspond to mudflats in the predam estuary. A reduction of the shallower depths and increase in deeper depths from the lake to the restored estuary indicate erosion of mudbanks and deepening of the channels after removal of the dam

the use of the morphological tide in the sediment transport simulations to reduce computational time for the long-term simulations. While the benefits of coupling the complexity of the semidiurnal tide with flood events has not been examined,

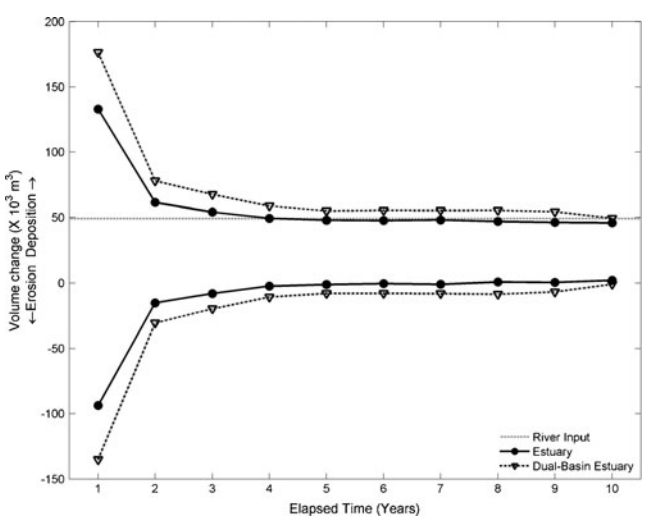

Fig. 12 Annual volume change ($\times 10^3$ m^3) in the Deschutes estuary and Budd Inlet for the estuary alternative (*circles*) and dual basin estuary alternative (*triangles*) for 10-year morphological simulations. Negative numbers indicate erosion, and positive numbers indicate accretion. The dual basin estuary exports sediment that would accumulate in eastern North Basin, which accounts for the larger volume changes. Both indicate large shifts in the first years after dam removal but gradual decreases through time as the rate of volume change asymptotically approaches the amount of sediment delivered by the river

aligning the river discharges at particular stages of the tide to statistical significance could prove to be unachievable. Recently, attempts have been made to combine and scale the two largest tidal constituents, which in this case would be the M2 and K1, but the impact on morphological change has not yet been elucidated (Lesser 2010). A second limitation in this category is the averaging of historical conditions. The Deschutes River hydrograph was deconstructed to reduce the high frequency noise of the data and produce a representative climate. In a standard assumption in forecast numerical modeling, the range of future conditions was conjectured to resemble those from the historical past. Another approach could have been to explore the effects of extreme conditions of flooding and drought on the morphological response.

The second of the Haff (1996) uncertainty categories relevant for this study is unknown initial conditions. The mud erodibility measurements from the Sedflume provided important constraints for the range of natural erodibilities found in the estuary. The findings allowed more certainty than estimates from published literature, but variability still exists in the natural environment. Primary sources of variability include the physical properties of the sediment, such as sediment grain size and water content (Postma 1967), and biological activity depending on how organisms disturb the bed (Jumars and Nowell 1984). While the physical properties of sediment typically vary across large spatial and temporal scales, the effect from biological activity has been observed to be localized and ephemeral (Wheatcroft and Butman 1997). As a result, marine sediments with similar properties can respond differently because of a biological overprint. Hence, a variety of erodibilities could coexist within a restored estuary, producing different results from those examined above. Sediment erodibility will also change through time from physical habitat changes coupled to shifting biological communities. For example, freshwater organisms will be replaced with euryhaline or marine organisms as the environment shifts from freshwater to brackish conditions. Another important limitation in this category is the use of a potentially obsolete sediment rating curve for the Deschutes River. The rating curve applied for sediment delivery was calculated in the 1970s during different usage of the watershed, including a larger intensity of logging. Urbanization, irrigation, and other anthropogenic activities have affected the river sediment load in unknown ways. A new rating curve based on modern flow and sediment discharge events would provide a better estimate of the present sediment load to the lake and possible future estuary.

Model Sensitivity to Sediment Type and Erodibility Parameters

Sediment transport links the hydrodynamics and morphodynamics in both the conceptual and the numerical models. As such, the sensitivity of the numerical model to sediment type

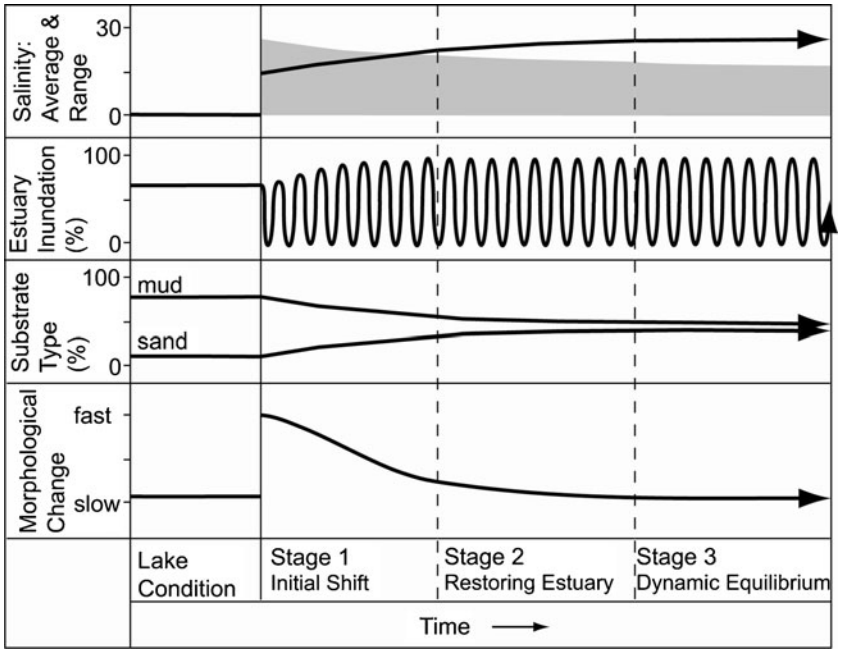

Fig. 13 Conceptual model of the process of estuary restoration according to various parameters describing the physical habitat. The three stages are an initial shift, a restoring estuary, and dynamic equilibrium, with time in ambiguous units. The salinity range decreases through time even as the average salinity increases from a deepening estuary. The inundation fraction, while dependent on the tidal stage, gradually increases as unstable mudbanks are eroded away. Substrate sediment distributions shift rapidly initially from a muddy bed to a more even distribution of sand and mud, although the actual fractions will depend on weathering in the watershed and sediment delivery to the estuary. The rate of morphological change, a large indicator of the progress of restoration, is initially rapid but decreases with time as the estuary evolves toward a balance with the tidal dynamics. All of these processes will continue through time and would be expected to respond to external forces such as climate change, sea level rise, and landscape alterations

and properties was investigated to examine how much these parameters control the results.

Sediment Type

For the sediment transport and morphological simulations, four representative sediment sizes were selected based on sediment collected from the lake bed (Table 6). Holding these classes as a base case, three additional sets of sediment classes were assembled to investigate differences in performance and results of the model (Table 9). The sediment in the multiple grain size test cases was selected to be representative of the mixed bed observed in field data, while in the single grain size test case, 35 μm was used to signify the general muddiness of the estuary. All four cases were run for 3 years on the estuary alternative model with identical parameters as the base case except for the sediment classes.

Cross-sections of the evolved bed morphology were compared among the base case and the test cases with particular attention given to the depth and position of the channels, and the height of the mudflats (Fig. 14, Appendix). Overall, the multiple grain size simulations (base case, test cases 1 and 2) show similar morphology across the mudflats and channels with average depth differences of 0.48 m±0.31 and horizontal offsets of identical depths of 15 m±9. Qualitatively, the shape of the cross-sections for these three cases shows gradual transitions from mudflats and to channels. In addition, multiple channels are formed near the mouth of the estuary in all three cases. Dispersion of sand and gravel into high-energy zones and silt and clay into low-energy zones was similar. Cross-sections from test case 3 (single grain size) are markedly different from the other cases. In seven of eight cross-sections, the thalweg in test case 3 was deeper, particularly at the highest velocity areas (e.g., 3–4 m deeper). Other cross-sections show an average depth difference of 1 m±0.48, while horizontal offsets of identical depths average 28 m±12. Deeper, leveed channels formed in test case 3 in locations where multiple shallower channels formed in the other cases; all of the mudflats are shallower in test case 3. While the amount of sediment deposited seaward is comparable, the resulting channels are more confining to the flow and do not broaden during the same time frame as the other test cases or basecase. The differences suggest a singular grain size simulation is less dispersive and more resistant to sediment remobilization.

While many lessons for modeling estuary evolution can be drawn from the sediment type analysis, two will be highlighted related to using multiple grain sizes. First, characterization and incorporation of local bed sediment is essential to reflect the possible outcomes. In this study, the bed sediment grain

Table 9 Representative sediment grain sizes used for model sediment type sensitivity analysis

Sediment type (μm)	Base case (4 classes)	Test case 1 (4 classes)	Test case 2 (7 classes)	Test case 3 (1 class)
Clay fraction	2	4	2 and 4	–
Silt fraction	31	15	15 and 31	35[a]
Sand fraction	200	300	200 and 300	–
Gravel fraction	2,000	2,000	2,000	–

[a] Test case 3 simulated all sediment as a mud fraction

size distribution is very poorly sorted, which necessitated using multiple sediment types. As seen with test case 3, a singular grain size bed produced incongruent results from other iterations, especially in the formation of multiple channels. Second, interaction among the multiple grain sizes is more reflective of natural processes and allows improved bed mobility. Preferential removal of fine sediment from sandy mixtures can redistribute the sediment classes spatially, which has been observed in field studies (e.g., Sanford 2008; Law et al 2008). The sorting of the sediment classes through varying shear stresses causes a morphological response. The large morphological differences between the three multiple grain size and single grain cases can be attributed to the absence of bed armoring in test case 3.

Mud Erodibility Parameters

The erosion rates measured in the Capitol Lake cores are typical of muddy depositional sediments measured in other areas with Sedflume (e.g., Lick et al. 1997). To examine the model sensitivity to differing mud erodibility, the variability of dry sediment density, critical shear stress, and erosion rate was statistically characterized as the mean value of the observed erodibility parameters ±1 standard deviation (Table 10). This yielded a range in erodibility parameters larger than the range of values found in the literature. The most likely combinations of the three parameters were chosen by analyzing the field data with a Bayes network (Spiegelhalter et al. 1993) with the computer program Netica. The Bayes network uses probabilistic inference to determine the relationships between each of the erodibility parameters and calculates the probability of occurrence based on the field data for the 27 possible combinations. The Bayes network analysis determined that the most likely combination of erodibility parameters (~14 % probability) occurs with a medium dry sediment density (455 kg m^{-3}), a medium critical shear stress (0.48 Pa), and a medium erosion rate parameter (3.93×10^{-3} kg m^{-2} s^{-1}); this combination was used in the morphological modeling discussed above. However, 13 other combinations could occur 4–10 % of the time and were tested in multiyear simulations.

The morphological change that occurs in the simulations is highly variable over the range of erodibility parameters applied in the model. The volume of sediment that accumulates seaward of the estuary after 3 years ranges 11×10^4–71×10^4 m^3 within the 14 erodibility parameter combinations; other portions of the estuary show comparable ranges for eroded sediment volumes. Overall, and not surprisingly, the combinations of low dry sediment density, low critical shear stress, and high or medium erosion rates generate the most mobilized sediment. Conversely, combinations with a more resistant bed (medium or high dry sediment density, medium or high critical shear stress, and medium erosion rate) produce the least amount of sediment transported in the estuary. This analysis is instructive for why constraining the erodibility parameters is necessary when modeling muddy environments that are out of equilibrium. The responsiveness of a model to field data-bounded input should be investigated for most studies to identify the possible range of outcomes. Those ranges may have a sizeable impact on decisions as well as contribute to broader understanding of modeling bed morphology.

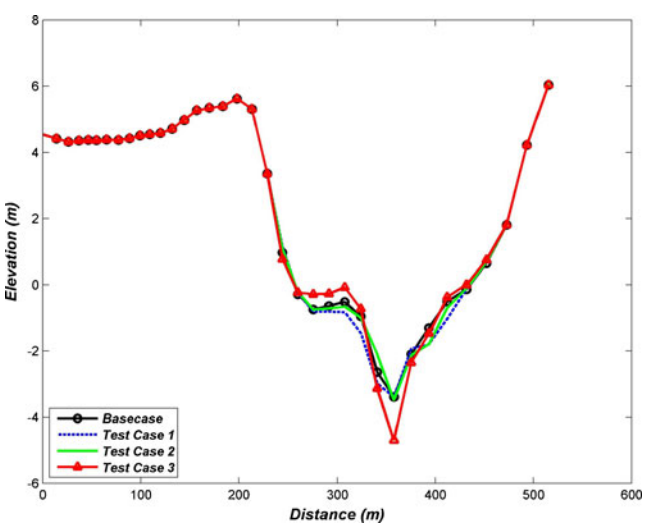

Fig. 14 Representative cross-section from sensitivity analysis to sediment grain size. See Table 9 for descriptions of sediment types used in the sensitivity analysis. The multiple grain size cases (*base case*, *test case 1*, and *test case 2*) produce more similar morphology than the single grain size case (*test case 3*), demonstrating the need for modeling multiple grain sizes in mixed bed environments. See Appendix for comparison of all eight cross-sections

Summary

A process-based hydrodynamic and sediment transport model was used to investigate decadal estuary evolution in a severely perturbed environment. Some of the metrics used included circulation patterns, wetting and drying,

Table 10 Erodibility parameters calculated from field data: the high and low values represent the mean value plus or minus one standard deviation for each parameter, respectively

Parameter	Low	Medium	High
Dry sediment density (kg m^{-3})	316	455	594
Critical shear stress (Pa)	0.18	0.48	0.78
Erosion rate parameter (kg m^{-2} s^{-1})	0.001	0.00393	0.0147

salinity regime, sediment transport, and morphological change that would occur with the restoration of tidal processes to an estuary. Hydrodynamics were simulated in 3D and sediment transport and morphological change in 2D. The development of decadal morphological simulations of the restored estuary required simplifying several data inputs and implementing a time-scale acceleration technique. The river sediment discharge was schematized to connect with morphological changes in the estuary. To reduce the computational time of the simulations, a variable morphological factor was employed, which is a scaling factor that relates the hydrodynamic time scale to the morphological time scale. Four sediment classes (2, 31, 200, and 2,000 μm) were used to represent the observed mixed bed and fluvial sediment and erodibility of the sediment was parameterized by laboratory analysis on sediment cores taken in the modern lake. Statistical analysis with a Bayes network of combinations of erodibility parameters (dry sediment density, critical shear stress, and erosion rate) refined the number of possible combinations from 27 to 14 based on the probability of occurrence.

The results were investigated in terms of how the physical habitat (bathymetry, substrate, inundation frequency, mean salinity, and salinity range) and morphology evolved through time. The estuary transitioned through multiple phases and approached dynamic equilibrium within a decade. The evolved estuary showed many bathymetric similarities with the predam estuary, allowing speculation that a functional estuary would develop should tidal forces be restored. The numerical model provided a tool to compare the functions of the historical estuary and alternatives for a restored estuary. The sensitivity of the morphological model to sediment types and erodibility parameters suggests that quantifying local sediment grain size distribution and erodibility are essential to constrain these uncertainties as much as possible. Using these findings as a guide, a conceptual model of the three stages of estuary evolution for a perturbed system was proposed. The conceptual model is useful in setting expectations for how a restored environment will evolve through time rather than remain a static ecosystem.

Acknowledgments This work was part of a large collaborative process, and we would like to acknowledge the contributions of the Deschutes Estuary Feasibility Study Technical Committee, including Curtis Tanner, Steven Morrison, and Nathaniel Jones. Giles Lesser was instrumental in developing the morphological modeling techniques. We thank Edwin Elias, Jodi Eshleman, and Bert Jagers for their assistance in executing the project. We thank George Tate and Craig Jones for help collecting cores and performing SedFlume analysis. Nathaniel Plant provided guidance in applying the Bayesian model to the erodibility data. The manuscript was greatly improved by input from Jessica Lacy, Greg Hood, Neil Ganju, and an anonymous reviewer. This project was funded by the Salmon Recovery Funding Board (SRFB), the Washington Department of General Administration, the Puget Sound Action Team, the Port of Olympia, and the US Geological Survey Coastal and Marine Geology Program. We thank our friends and colleagues for their support during this multiyear effort.

Appendix

Cross-Section Transects Used in Sensitivity Analysis to Sediment Grain Size

Fig. 15 Map of cross-section locations in model domain

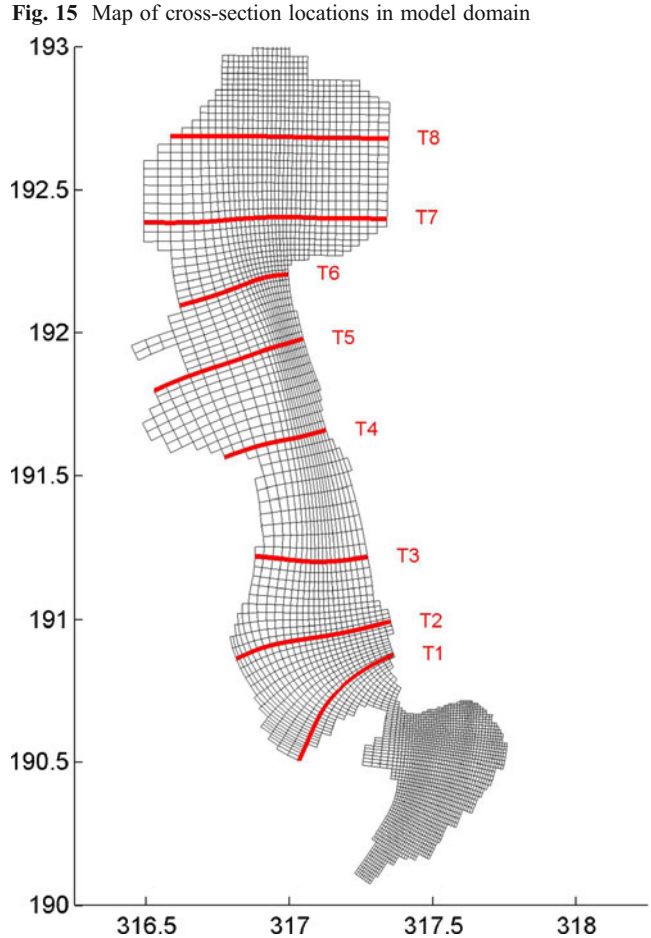

Fig. 16 Cross-section transect 1

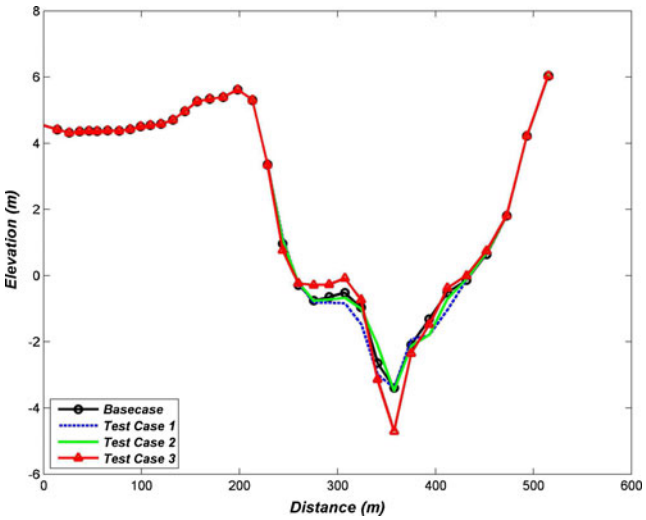

Fig. 17 Cross-section transect 2

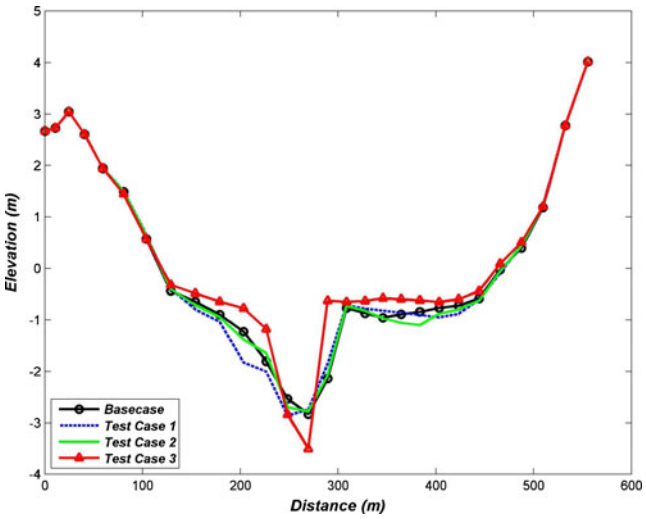

Fig. 18 Cross-section transect 3

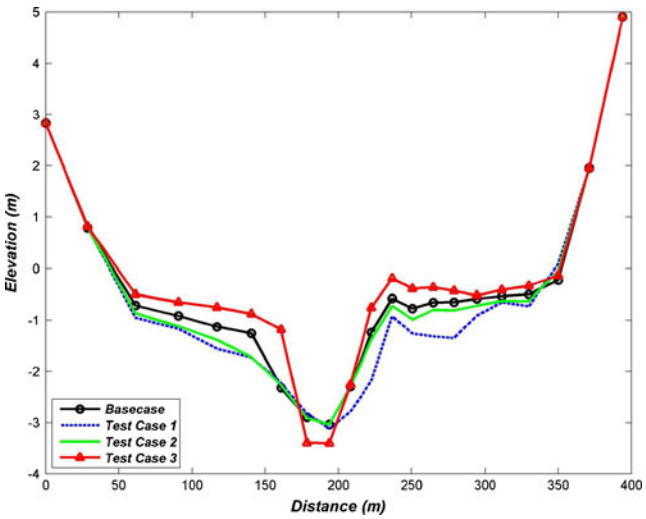

Fig. 19 Cross-section transect 4

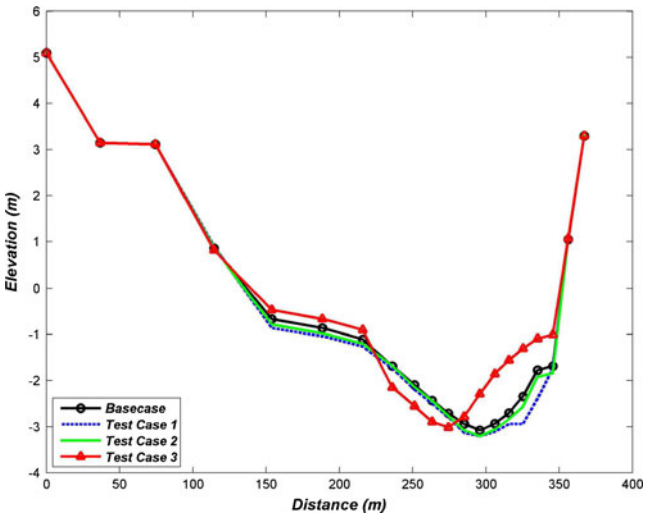

Fig. 20 Cross-section transect 5

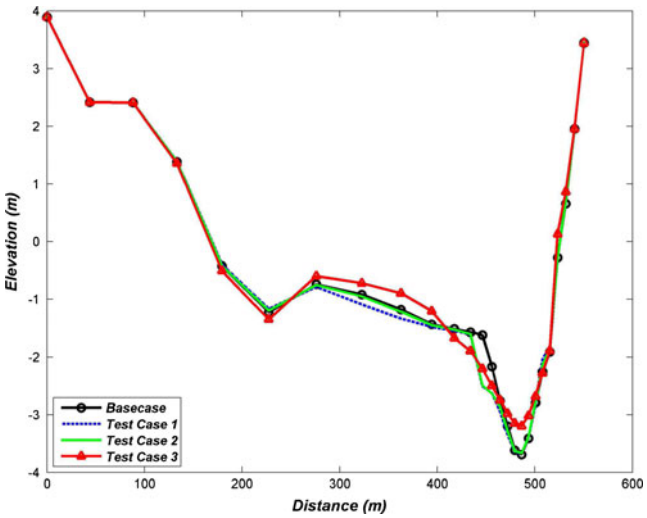

Fig. 21 Cross-section transect 6

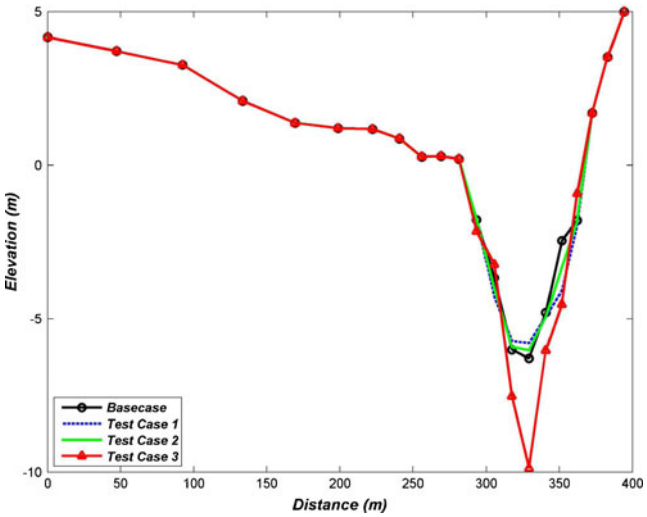

Fig. 22 Cross-section transect 7

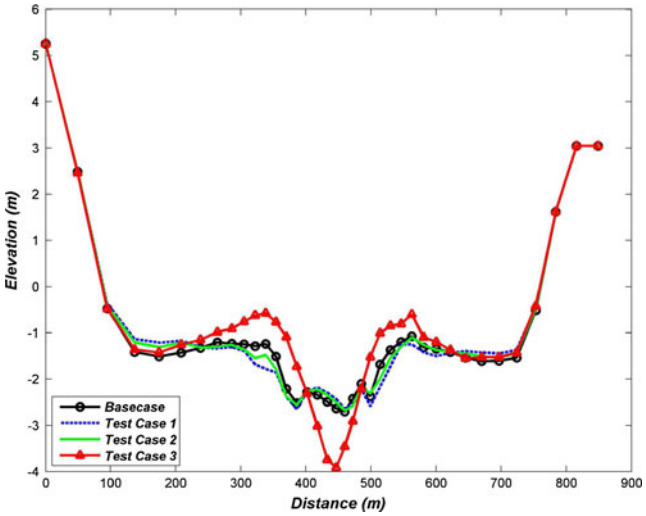

Fig. 23 Cross-section transect 8

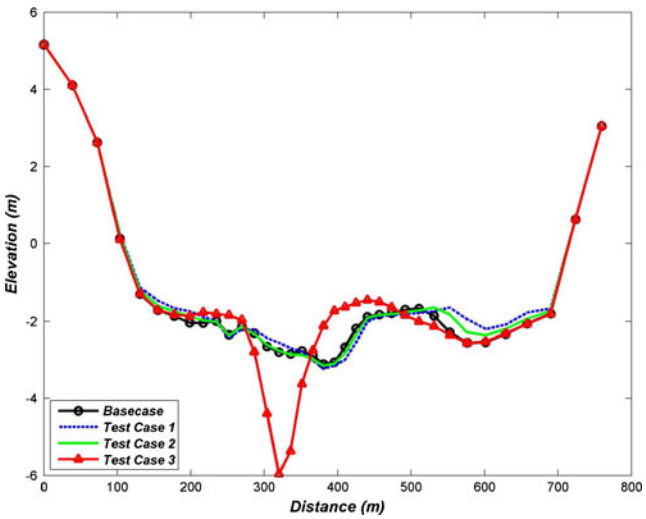

References

Cooper, J.A.G. 2002. The role of extreme floods in estuary-coastal behaviour: contrasts between river- and tide-dominated microtidal estuaries. *Sedimentary Geology* 150: 123–137.

Dalrymple, R.W., B.A. Zaitlin, and R. Boyd. 1992. Estuarine facies models: conceptual basis and stratagraphic implications. *Journal of Sedimentary Petrology* 62(6): 1130–1146.

Davis, R.A. (ed.). 1978. *Coastal sedimentary environments*, 413. New York: Springer.

De Vriend H.J., Capobianco M., Latteux B., Chesher T., Stive M.J.F., 1993. Approaches to long-term modelling of coastal morphology: A review. *Coastal Engineering* 21: 225–269.

Eshleman, J., Ruggiero, P., Kinsley, E., Gelfenbaum, G., and George, D., 2006. Capitol Lake, Washington 2004 data summary. USGS Data Series report.

Friedrichs, C.T., and D.G. Aubrey. 1996. Uniform bottom shear stress and equilibrium hypsometry of intertidal flats, in mixing in Estuaries and Coastal Seas. *Coastal and Estuarine Studies* 50: 405–429.

Ganju, N.K., N. Knowles, and D.H. Schoellhamer. 2008. Temporal downscaling of decadal sediment load estimates to a daily interval for use in hindcast simulations. *Journal of Hydrology* 349: 512–523.

Gelfenbaum, G., Roelvink, J.A., Meijs, M., Buijsman, M. and Ruggiero, P. 2003. Process-based morphological modeling of Grays Harbor inlet at decadal timescales. Proceedings of the Coastal Sediments '03 International Conference, 13p.

George, D. A., Gelfenbaum, G., Lesser, G., Stevens, A. W. 2006. Deschutes estuary feasibility study—Hydrodynamics and sediment transport modeling. United States Geological Survey Open File Report 2006–1318. 222 pp.

Haff, P.K. 1996. Limitations on predictive modeling in geomorphology. In *The scientific nature of geomorphology*, ed. B.L. Rhoads and C.E. Thorn, 337–358. New York: Wiley.

Hill, P.S. 1998. Controls on floc size in the sea. *Oceanography* 11: 13–18.

Jumars, P.A., and A.R.M. Nowell. 1984. Effects of benthos on sediment transport: difficulties with functional grouping. *Continental Shelf Research* 3: 115–130.

Latteux, B. 1995. Techniques for long-term morphological simulation under tidal action. *Marine Geology* 126: 129–141.

Law, B.A., P.S. Hill, T.G. Milligan, K.J. Curran, P.L. Wiberg, and R.A. Wheatcroft. 2008. Size sorting of fine-grained sediments during erosion: results from the western Gulf of Lions. *Continental Shelf Research* 28(15): 1935–1946.

Lesser, G. R. 2010. An approach to medium-term coastal morphological modeling. UNESCO-IHE PhD thesis. UNESCO-IHE Institute for Water Education, Delft, The Netherlands.

Lesser, G.R., J.A. Roelvink, J.A.T.M. Van Kester, G.S. Stelling, and V. Lakhan. 2004. Development and validation of a three-dimensional morphological model. *Coastal Engineering* 51: 883–915.

Lick, W., Z. Chroneer, C. Jones, and R. Jepsen. 1997. A predictive model of sediment transport. *Estuarine and Coastal Modeling* 5: 389–399.

Mathews, R., and B.D. Richter. 2007. Application of the indicators of hydrologic alteration software in environmental flow setting. *Journal of the American Water Resources Association* 43: 1400–1413.

McNeil, J., C. Taylor, and W. Lick. 1996. Measurements of erosion of undisturbed bottom sediments with depth. *Journal of Hydraulic Engineering* 122: 316–324.

Mih, W., and J. Orsborn. 1974. *Sediment removal and maintenance system for the upper basin of Capital Lake Olympia, Washington. Preliminary Report*, 33. Pullman: Washington State University.

Partheniades, E. 1965. Erosion and deposition of cohesive soils. *Journal of the Hydraulics Division, American Society of Civil Engineers* 91: 105–138.

Postma, H., 1967. Sediment transport and sedimentation in the estuarine environment. In *Estuaries*, ed. G.H. Lauff, 158–179. Washington: AAAS.

Pritchard, D., A.J. Hogg, and W. Roberts. 2002. Morphological modeling of intertidal mudflats: the role of cross-shore tidal currents. *Continental Shelf Research* 22: 1887–1895.

Roberts, J., R. Jepson, D. Gotthard, and W. Lick. 1998. Effects of particle size and bulk density on erosion of quartz particles. *Journal of Hydraulic Engineering* 124: 1261–1267.

Roberts, W., P. Le Hir, and R.J.S. Whitehouse. 2000. Investigation using simple mathematical models of the effect of tidal currents and waves on the profile shape of intertidal mudflats. *Continental Shelf Research* 20(10/11): 1079–1097.

Roelvink, J.A. 2006. Coastal morphodynamic evolution techniques. *Coastal Engineering* 53: 277–287.

Sanford, L.P. 2008. Modeling a dynamically varying mixed sediment bed with erosion, deposition, bioturbation, consolidation, and armoring. *Computers and Geosciences* 34(10): 1263–1283.

Simenstad, C., D. Reed, and M. Ford. 2006. When is restoration not? Incorporating landscape-scale processes to restore self-sustaining ecosystems in coastal wetland restoration. *Ecological Engineering* 26(1): 27–39.

Sondi, I., M. Juracic, and V. Pravdic. 1995. Sedimentation in a disequilibrium estuary: the Rasa River Estuary (Adriatic Sea, Croatia). *Sedimentology* 42: 769–782.

Soulsby, R.L., L. Hamm, G. Klopman, D. Myrhaug, R.R. Simons, and G.P. Thomas. 1993. Wave–current interaction within and outside the bottom boundary layer. *Coastal Engineering* 21: 41–69.

Spiegelhalter, D.J., A.P. Dawid, S.L. Lauritzen, and R.G. Cowell. 1993. Bayesian analysis in expert systems. *Statistical Science* 8: 219–293.

Stevens, A.W., R.A. Wheatcroft, and P.L. Wiberg. 2007. Seabed properties and sediment erodibility along the western Adriatic margin. *Italy: Continental Shelf Research* 27: 400–416.

Stevens, A.W., Gelfenbaum, G., Elias, E., Jones, C., 2008. Incorporation of fine-grained sediment erodibility measurements into sediment transport modeling, Capitol Lake, Washington. US Geological Survey Open-File Report 2008–1340, 72 p.

Uncles, R.J. 2002. Estuarine physical processes research: some recent studies and progress. *Estuarine, Coastal and Shelf Science* 55: 829–856.

van der Wegen, M., A. Dastgheib, B.E. Jaffe, and D. Roelvink. 2010. Bed composition generation for morphodynamic modeling: case study of San Pablo Bay in California, USA. *Ocean Dynamics* 61 (2–3): 173–186.

van der Wegen, M., B.E. Jaffe, and D. Roelvink. 2011. Process–based, morphodynamic hindcast of decadal deposition patterns in San Pablo Bay, California, 1856–1887. *Journal of Geophysical Research* 116: F02008. doi:10.1029/2009JF001614.

van Rijn, L. 1993. *Principles of sediment transport in rivers, estuaries, and coastal seas*, 715. Amsterdam: Aqua.

Wheatcroft, R.W., and C.A. Butman. 1997. Spatial and temporal variability in aggregated grain-size distributions, with implications for sediment dynamics. *Continental Shelf Research* 17: 367–390.

Williams, P.B., M.K. Orr, and N.J. Garrity. 2002. Hydraulic geometry: a geomorphic design tool for tidal marsh channel evolution in wetland restoration projects. *Restoration Ecology* 10(3): 577–590.

Wood, R., and J. Widdows. 2002. A model of sediment transport over an intertidal transect, comparing the influences of biological and physical factors. *Limnology and Oceanography* 47: 848–855.